Scientia Iranica A (2017) 24(6), 2803–2816

Sharif University of Technology
Scientia Iranica
Transactions A: Civil Engineering
www.scientiairanica.com

Evaluation of behavior of bucket foundations under pure loading

V. Ghaseminejad[a,*] and M.A. Rowshanzamir[b]

a. *Department of Civil Engineering, Isfahan (Khorasgan) Branch, Islamic Azad University, Isfahan, Iran.*
b. *Department of Civil Engineering, Isfahan University of Technology, Isfahan, Iran.*

Received 27 December 2015; received in revised form 17 May 2016; accepted 16 August 2016

KEYWORDS
Offshore wind turbines;
Bucket foundations;
Finite-element analyses;
Pure bearing capacity;
Medium-dense sand.

Abstract. Offshore wind turbine as a green renewable resource can have important roles in changing energy structure. In this study, the results of three-dimensional finite-element analyses of the pure horizontal, vertical, and moment loading of bucket foundations in medium-dense sand are presented. Sensitivity analyses have been performed on different bucket diameters and length-to-diameter aspect ratios (L/D); the responses for pure horizontal, vertical, and moment loading have been compared with each other. To determine the pure horizontal, vertical, and moment-bearing capacities of the bucket foundation, different methods have been compared. Charts and functions derived from finite-element results and responses are presented as failure envelopes in $M-H$ plane. The results show that pure ultimate capacity of the bucket significantly depends on bucket geometry and aspect ratio.

1. Introduction

Selecting the type of foundation depends on the site and is greatly affected by both soil properties and the environment. Foundations of offshore structures make their contribute to carry large horizontal loads and bending moments because wind, waves, and current forces act laterally on the superstructure, vertical load of the superstructure weight, and foundation system itself in order to be safely transferred to the sea ground. Bucket foundations have been found attractive, firstly due to their convenient method of installation and repeated use and, secondly, due to their capability of mobilizing a significant amount of reverse-end bearing or passive suction during uplift. Bucket foundations are often used in shallow water depths from near shore to approximately 55 m far. A bucket foundation is a circular foundation with thin skirts around its circumference consisting of a large steel cylindrical shaft of diameter D, skirt length L, and skirt thickness t_s, with a closed top and open bottom. They first penetrate into the seabed usually under their weight beneath the base plate, which is confined to a soil plug. Further penetration will take place by pumping water out of the bucket foundation, which can create a suction pressure inside it. Penetration will stop when the top plate of the bucket approaches the seabed.

Offshore wind turbines are light and dynamically sensitive structures. Loads from offshore wind turbines are characterized by a unique loading condition that consists of horizontal forces, including a heavy overturning moment with yet relatively low vertical loads because of their slender construction. Understanding the behavior of shallow foundations subjected to combined loads is considerably important for geotechnical engineers. Some applications of offshore shallow foundation systems are illustrated in Figure 1. In deeper

*. *Corresponding author. Tel.: +98 1132217685; Fax: +98 1132231911*
E-mail addresses: vghaseminejad@gmail.com (V. Ghaseminejad); mohamali@cc.iut.ac.ir (M.A. Rowshanzamir)

doi: 10.24200/sci.2017.4166

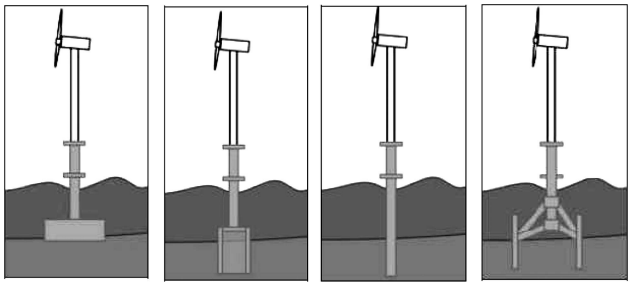

Figure 1. Different types of offshore wind turbine foundations from left to right: gravity base, bucket foundation, monopile foundation, and tripod foundation with piles [1].

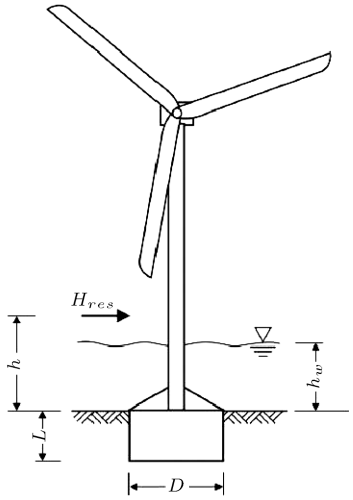

Figure 2. Sketch of bucket foundation of offshore wind turbines [2].

water depths, the gravity of the foundation may be replaced by a monopile, a bucket foundation, or a jacket structure.

A general sketch of a typical offshore wind turbine with a bucket foundation is shown in Figure 2. To install, an underpressure is applied to the cavity between the top plate and seabed (Figure 3).

2. Literature review

In November 2002, the first bucket foundation for a wind turbine was installed at the offshore test facility in Frederikshavn that was the largest wind turbine at the time. The skirt length and diameter of the bucket foundation were equal to 6 m and 12 m, respectively, i.e. $L/D = 0.5$ [1]. Cassidy et al. [4], Houlsby and Cassidy [5], and Cassidy [6] described a work-hardening plasticity criterion for the behavior of rigid circular foundations resting on loose carbonate sand, when subjected to combined loading. Gourvenec and Randolph [7,8] and Bransby and Yun [9] presented the results of two- and three-dimensional finite-element analyses of the combined loading of strip and circular skirted footings installed in homogeneous and non-homogeneous clay and investigated the ultimate limit states and failure envelopes. Gerolymos and Gazetas [10,11] developed a nonlinear Winkler-spring method for the static, cyclic, and dynamic responses of caisson footings. Bienen et al. [12] carried out an experimental study using a loading device that applied general loading to a model with shallow foundations. Kelly et al. [13] conducted laboratory tests applying vertical and moment loads to suction caissons installed in sand and clay to simulate an equivalent series of field tests. Vertical load tests in sand have been performed using 0.15 m and 0.2 m diameter buckets in the laboratory to compare with a 1.5 m diameter bucket (aspect ratio of 0.66) in the field. Moment load tests in sand were conducted using buckets with diameters of 0.2 m and 0.3 m in the laboratory and 3.0 m diameter (aspect ratio of 0.5) in the field. Gourvenec [14,15] compared the ultimate limit states under combined loading of rectangular foundations with varying aspect ratios. Gourvenec [16] evaluated the effect of embedment on the undrained bearing capacity of shallow strip footings under uniaxial load and combined loading from a finite-element study. Bienen et al. [17] established the undrained ultimate load capacity of a circular skirted foundation under uniaxial horizontal and moment loading. Gerolymos et al. [18] and Gerolymos and Gazetas [19] investigated the undrained behavior of massive caisson foundations towards the combined loading from a series of three-dimensional finite-element analyses. Hung and Kim [20] described the results of three-dimensional finite-element analyses of suction buckets installed in normally consolidated uniform clay subjected to undrained conditions. Abdel-Rahman and Achmus [21] investigated the response of the monopile and the

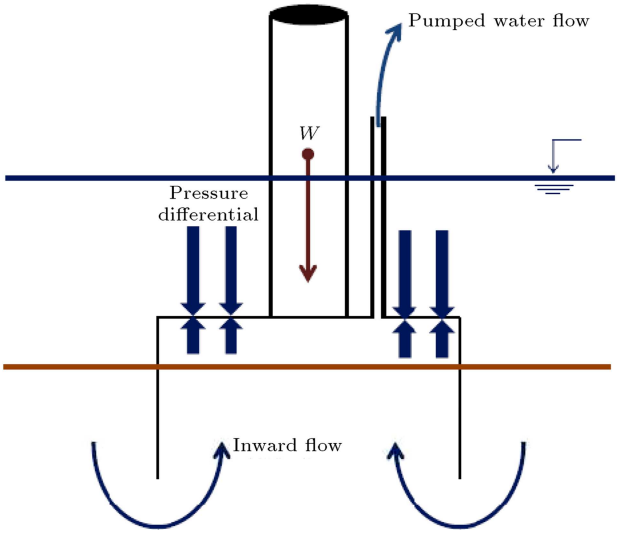

Figure 3. Bucket foundation during installation by suction [3].

bucket foundation under monotonous loading taking the interaction between the foundation system and the subsoil into account. Panayides et al. [22] developed the results of a numerical study into the bearing capacity and failure mechanisms of suction caissons founded in structured clays using an advanced soil constitutive model. Larsen et al. [23] investigated the behavior of suction buckets with varying sizes, aspect ratios, and load paths under combined loads using the results of experimental studies on the saturated dense Aalborg University Sand. Foglia et al. [24] formulated and validated a macro-element model for suction buckets against small-scale experimental results. Ibsen et al. [25,26] developed a new strain-hardening model by calibrating failure criteria and employing the data from small-scale tests on bucket foundations under static loads. An extensive number of combined loading tests with small-scale bucket footings were implemented in the laboratory at Aalborg University in Denmark. These tests were conducted on buckets with varying sizes, aspect ratios, and load paths. Barari and Ibsen [27-29] presented experimental and numerical results of vertical and moment loading on small-scale circular surface and suction bucket models on Baltic clay at Aalborg University. Ding et al. [30] conducted several field tests on the bearing capacity of Wide-Shallow Composite Bucket Foundations (WSCBF) for offshore wind turbines in saturated clay. Based on the position of the rotation center, analytical expressions of soil pressure and ultimate bearing capacity of the WSCBF were presented. Zhang et al. [31] carried out experimental work on installation of hybrid bucket foundations for offshore wind turbines in silty clay. Their results showed that suction can be combined with air pumping to reasonably control the sinking speed of the bucket foundation and the levelness at each stage.

In this study, the evaluations of the pure horizontal, vertical, and moment-bearing capacities of bucket foundations were performed using the results from finite-element analyses. The values were compared with each other, and finally, one of the methods was selected as a pure bearing capacity. The effects of diameter and aspect ratios on the pure bearing capacity of the bucket were parametrically investigated and charts and equations were presented. The sign conventions of loads and displacements are shown in Figure 4.

3. Validation of the numerical model

Finite-element analyses of bucket foundation founded in very dense sand performed by Achmus et al. (2013) [2] were simulated by three-dimensional finite-element program PLAXIS [32], and the results were validated. The details of the combined loading were reported in their study. A bucket foundation with a

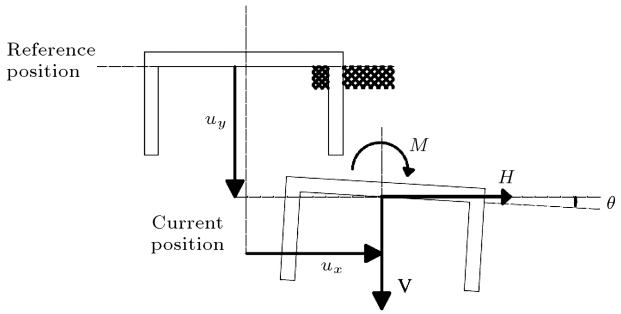

Figure 4. Sign conventions of loads and displacements of bucket.

Table 1. Soil parameters used by Achmus et al. [2] for the finite-element analysis in very dense sand.

Property	Value	Unit
Buoyant unit weight (γ')	11	(kN/m^3)
Oedometric stiffness parameter (κ)	600	–
Oedometric stiffness parameter (λ)	0.55	–
Poisson's ratio (ν)	0.25	–
Internal friction angle (φ')	40	(deg)
Dilation angle (ψ')	10	(deg)
Cohesion (C')	0.1	(kN/m^2)

diameter of $D = 12$ m, an aspect ratio of $L/D = 0.75$, and a skirt thickness of $t_s = 3$ cm was analyzed. Table 1 shows material parameters reported by Achmus et al. used in very dense sand. The comparison was performed for loading eccentricities of $h = 2.5$ and 100 m. The vertical load was considered $V = 10$ MN.

Horizontal load-displacement and moment-rotation curves were compared with the analysis performed by Achmus et al. [2], as shown in Figure 5. As can be seen, the numerical simulation results show good agreement with their findings.

4. Finite-element analyses

The three-dimensional finite-element program PLAXIS (3D version 1.6) [32] was used to evaluate the behavior of bucket foundation. Primary analyses were performed to determine mesh fineness in order to minimize the discretization error for each case and avoid the effect of boundary conditions. Then, a soil model whose length is 6 times the bucket diameter and a model whose depth is 3 times the bucket length were considered. Displacements at the bottom face nodes were fully fixed for x, y, and z directions. Normal displacements at side face nodes were constrained and fixed at horizontal displacement. Figure 6 shows a schematic of the finite-element mesh used in the current analyses. The elements used in the 3D finite-element calculations were 15 node triangular elements within PLAXIS. These were generated from the 6-

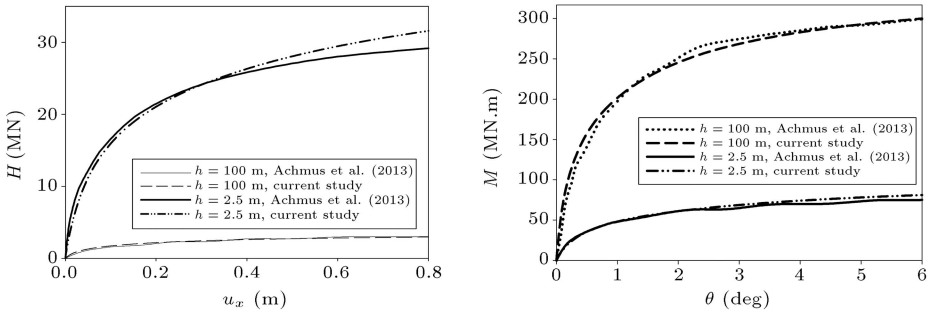

Figure 5. Horizontal load displacement and moment-rotation curves for the finite-element simulation in comparison with Achmus et al. [2] results.

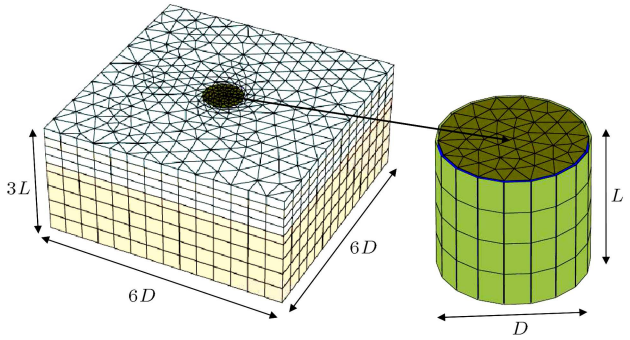

Figure 6. Finite-element mesh used in the analyses.

node triangular elements as generated in the 2D mesh, both the bucket foundation and the surrounding soil. An elastic-plastic model was used to describe the behavior between skirt and soil. The roughness of the interaction between the bucket surfaces and soil was modelled by choosing a suitable value for the strength reduction factor in the interface (R_{inter}). This factor relates the interface strength to the soil strength that is considered 0.7. Slipping, gapping, or overlapping between the bucket and surrounding soil was prevented. Both the bucket and soil were modelled with volume elements. The foundation was modelled as a rigid body.

In modeling bucket foundations, bucket diameters of $D = 8$ m, 12 m, 16 m, and 20 m, aspect ratios of $L/D = 0$, 0.25, 0.5, 0.75, and 1, and a skirt thickness of $t_s = 0.04$ m were examined. Actual steel deformation properties of $E = 210$ GPa and $\nu = 0.2$ were used, where E and ν represent the Young's modulus and Poisson's ratio of steel material, respectively. Submerged unit weight of the steel used for the bucket body was: $\gamma' = 68$ kN/m^3. A top-plate thickness of $t_L = 0.10$ m, unit weight $\gamma' = 77$ kN/m^3, and a very large modulus of elasticity $E = 1 \times 10^9$ Gpa were applied to the bucket lid. First, soil normal stresses in the model were only considered by the application of gravity loading. Subsequently, the elements defining the steel bucket were replaced by modeling the bucket foundation in the soil. Then, pure horizontal, vertical, and moment loads were separately applied to the bucket lid, increasing gradually until the pure bearing capacity of the bucket foundation was reached. Pure moment was applied by couple loads of eccentricity, h. As loading is stress controlled, pure vertical, horizontal, and moment loads on the bucket foundation were applied to the top of the bucket lid by a prescribed force at the center of the foundation. In the PLAXIS, the foundation soil is an elastic-plastic material obeying the Mohr-Coulomb failure criterion. As the modulus of elasticity of sand varies with depth, the non-uniformity of sand was considered using the following equation:

$$E_s = \kappa.\sigma_{at}.\left(\frac{\sigma_m}{\sigma_{at}}\right)^{\lambda}, \tag{1}$$

where $\sigma_{at} = 100$ kN/m^2 is reference stress, and σ_m is the current mean principle stress. Parameters κ and λ determine the soil stiffness at the reference stress state [2]. Table 2 gives material parameters used for medium-dense sand.

Table 2. Material parameters used for medium-dense sand.

Property	Value	Unit
Buoyant unit weight (γ')	16	(kN/m^3)
Saturated unit weight (γ_{sat})	19	(kN/m^3)
Oedometric stiffness parameter (κ)	400	–
Oedometric stiffness parameter (λ)	0.6	–
Poisson's ratio (ν)	0.25	–
Internal friction angle (φ')	35	(deg)
Dilation angle (ψ')	5	(deg)
Cohesion (C')	0.1	(kN/m^2)

5. Results and discussions

A method to estimate pure horizontal and ultimate moment capacities can be an extrapolation based on the hyperbolic method in which u_x/H with u_x and θ/M with θ relationships are used. Inverse slopes of the line in the charts could be taken as horizontal and moment-bearing capacities, respectively. Figure 7 presents the

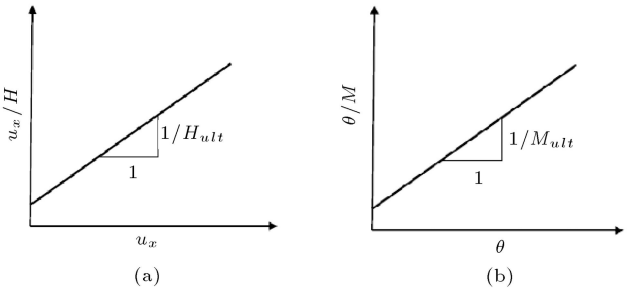

Figure 7. Hyperbolic method for the estimation of loading capacity as the inverse slope of the line: (a) u_x/H to u_x relationship, and (b) θ/M to θ relationship.

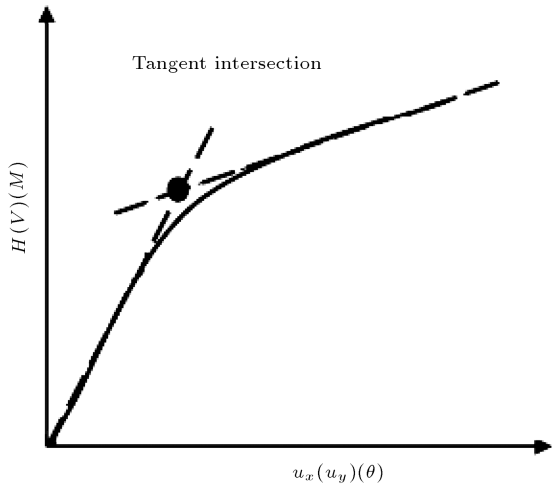

Figure 8. Tangent intersection method to estimate the ultimate capacity.

hyperbolic method to estimate the ultimate bearing capacity.

Another method for the estimation of pure horizontal, vertical and moment ultimate capacities can be tangent intersection method can also be used as an alternative to estimate pure horizontal, vertical, and ultimate moment capacities. In this method, horizontal, vertical, and ultimate moment capacities are defined as loads corresponding to the intersection point of two tangential lines along the initial and latter portions of the load-displacement curve (Figure 8). The method can be suitable for determining bearing capacity.

Limiting the displacement and rotation can be another option to estimate pure horizontal, vertical, and ultimate moment capacities.

Values of pure horizontal loads related to u_x/D of 5%, 7.5%, and 10%, rotations of 1, 2, 3 degrees, the tangent intersection method, and the hyperbolic relationship are presented in Figure 9. After comparing the methods, it was found that pure horizontal load at the rotation of 2° could be considered as the pure horizontal bearing capacity. Hyperbolic relationship, especially at higher diameters, showed the results different from those of the other methods. The method of limiting the horizontal displacement could not suitably estimate pure horizontal capacity in all cases at different diameters and aspect ratios.

Values of pure vertical loads related to u_y/D of 5%, 7.5%, and 10%, settlements of 20, 30, 50 cm, and tangent intersection method are illustrated in Figure 10. After comparing different methods, pure vertical load at settlement of 30 cm could be considered as pure vertical bearing capacity. Similar to the state of pure horizontal loading, the method of limiting the relative settlement (u_y/D) was not able to suitably estimate pure vertical capacity in all cases at different diameters and aspect ratios.

Deformations, particularly the limitation of the rotation of bucket foundation are significant for the design and serviceability of offshore wind turbines. Thus, a method to estimate ultimate moment-loading capacity could be limiting the rotation of bucket foundation. Values of pure moment loads related to rotations of $\theta = 0.5, 1, 2, 3$, and 4°, tangent intersection method, and hyperbolic relationship are presented in Figure 11. Due to the similarities between the results of tangent intersection method and that of 2° rotation, it seems reasonable to use the latter in order to determine pure moment-bearing capacity. Larsen (2008) [1] also found that a complete failure mechanism is developed approximately at a rotation of 2°.

Figure 12 shows a view of deformed finite-element mesh under pure horizontal loading at large deformations.

In pure horizontal loading, the coupling between the horizontal and rotational degrees of freedom played an important role, especially with increases in embedment ratios. Thus, the assumption of 2-degree rotation could be reasonable for the estimation of pure horizontal bearing capacity. Figure 13 displays pure horizontal load displacement to diameter ratio curves at different aspect ratios and diameters.

Horizontal bearing capacity decreased as aspect ratio (L/D) and bucket diameter (D) declined. The decreasing rate of horizontal capacity varied between 14% and 20% from $L/D = 1$ to 0.75; 11% and 24% from $L/D = 0.75$ to 0.5; 41% and 53% from $L/D = 0.5$ to 0.25; and 67% and 86% from $L/D = 0.25$ to 0 at different diameters.

The pure vertical bearing capacity of bucket indicates the governing loading conditions of the structure due to its weight. Figure 14 shows a view of the deformed finite-element mesh under pure vertical loading.

Failure under pure vertical loads was almost governed by pure vertical translations. Therefore, assuming a 30 cm settlement could be reasonable to estimate pure vertical capacity. Figure 15 displays

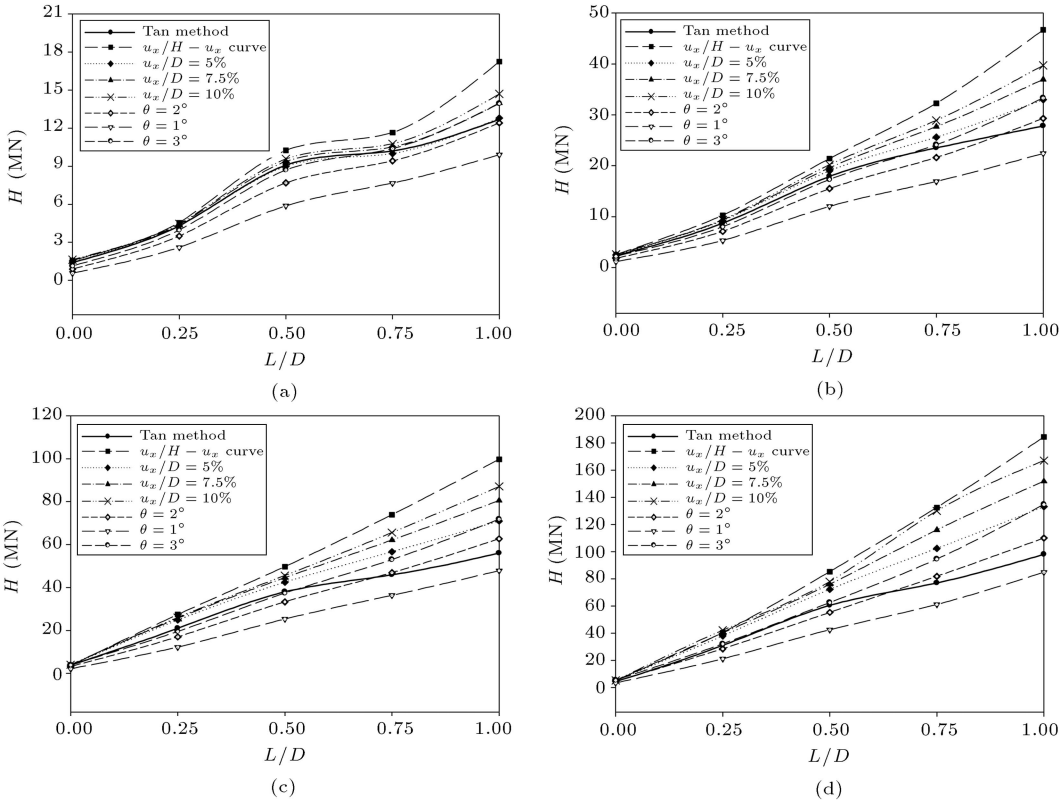

Figure 9. Comparison of different methods to estimate suitable pure horizontal capacity: (a) $D = 8$ m, (b) $D = 12$ m, (c) $D = 16$ m, and (d) $D = 20$ m.

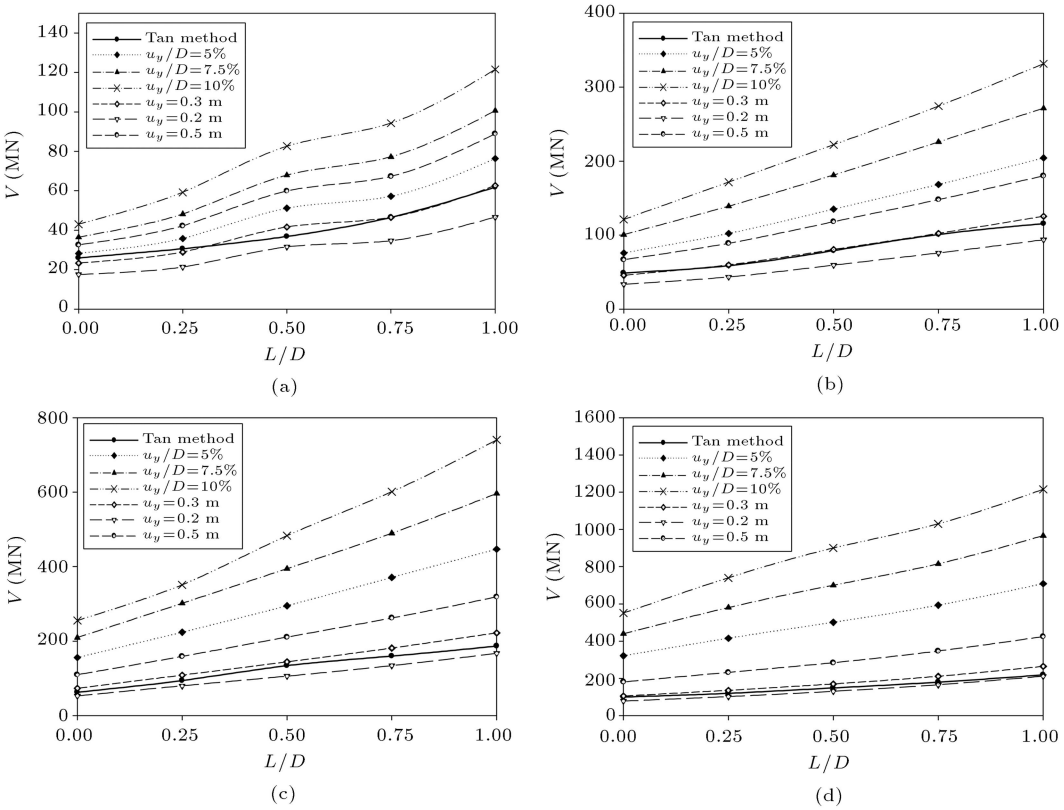

Figure 10. Comparison of different methods to estimate suitable pure vertical capacity: (a) $D = 8$ m, (b) $D = 12$ m, (c) $D = 16$ m, and (d) $D = 20$ m.

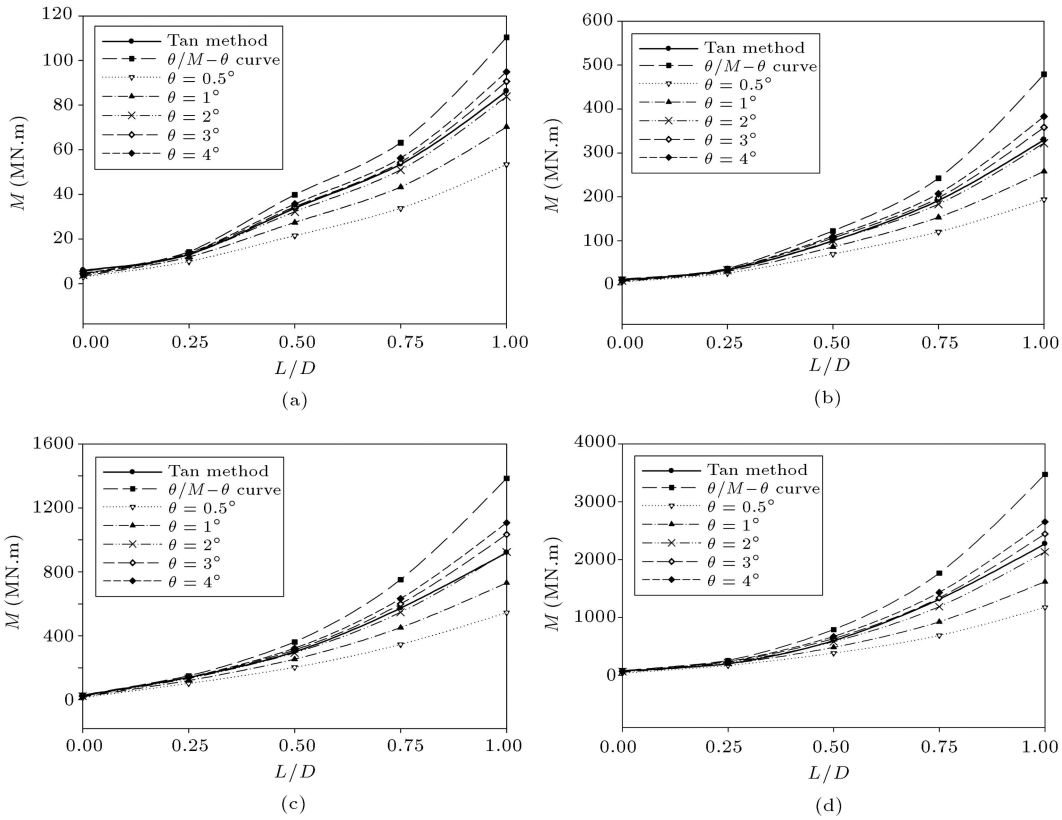

Figure 11. Comparison of different methods to estimate suitable pure moment capacity: (a) $D = 8$ m, (b) $D = 12$ m, (c) $D = 16$ m, and (d) $D = 20$ m.

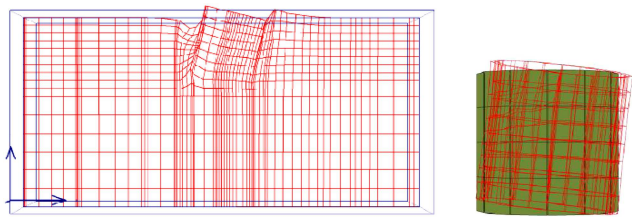

Figure 12. Deformed finite-element mesh in pure horizontal load at large deformations.

settlement to diameter ratio and pure vertical load curves at different aspect ratios and diameters.

A decrease in the aspect ratio (L/D) led to a fall in vertical bearing capacity. Vertical bearing capacity increased as bucket diameter went up. The decreasing rate of the vertical capacity was variable between 13% and 25% from $L/D = 1$ to 0.75; 16% and 22% from $L/D = 0.75$ to 0.5; 14% and 30% from $L/D = 0.5$ to 0.25; and 15% and 33% from $L/D = 0.25$ to 0 at different diameters.

A pure rotation would not accompany failure under pure moment, because the coupling between the horizontal and rotational degrees of freedom caused rotation and horizontal displacement when a moment load was applied at the foundation level. Under pure moment conditions, failure of bucket foundation occurred as the scoop of soil rotated beneath footing. Figure 16 shows a view of deformed finite-element mesh under pure moment loading at large deformations.

Moment-rotation relationships at different aspect ratios and diameters are shown in Figure 17.

Moment bearing capacity increased with an increase in aspect ratio (L/D) and also went up as the bucket diameter of each L/D ratio rose. The decreasing rate of the moment capacity was variable between 39% and 44% from $L/D = 1$ to 0.75; 37% and 51% from $L/D = 0.75$ to 0.5; 55% and 67% from $L/D = 0.5$ to 0.25; and 70% and 84% from $L/D = 0.25$ to 0 at different diameters.

The results showed that both horizontal and vertical displacements as well as rotation increased as horizontal, vertical, and moment loads rose until a clear ultimate load was reached. Subsequently, deformations increased with an almost horizontal line in the load-deformation curves.

It should be noted that variations in aspect ratios significantly affected pure ultimate loads. It was found that the lowest pure loading capacities (H_{ult}, V_{ult}, and M_{ult}) could be obtained at $L/D = 0$, and the highest pure loading capacity could be obtained at $L/D = 1$ at each diameter for $0 \leq L/D \leq 1$. Figure 18 shows pure horizontal, vertical, and moment-bearing capacities versus L/D curves.

To determine pure horizontal bearing capacity,

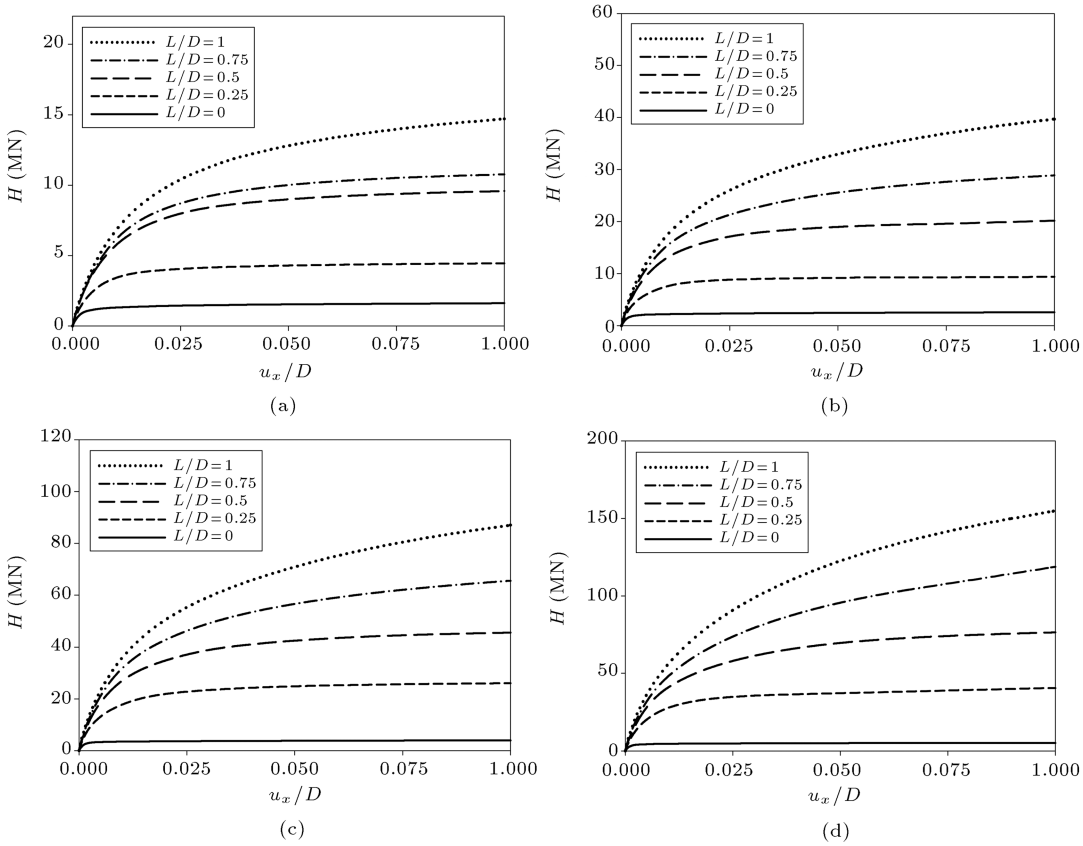

Figure 13. Pure horizontal load displacement to diameter ratio curves at different diameters: (a) $D = 8$ m, (b) $D = 12$ m, (c) $D = 16$ m, and (d) $D = 20$ m.

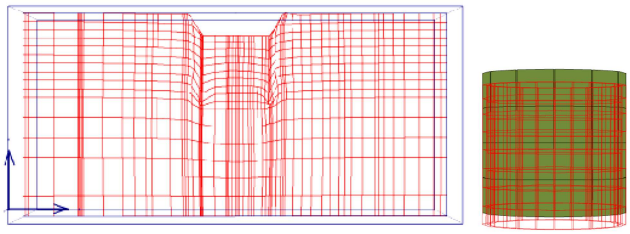

Figure 14. Deformed finite-element mesh in pure vertical load.

the following expression was found to be able to better match with the numerical results:

$$H_{ult} = a_H + b_H \left(\frac{L}{D}\right), \tag{2}$$

where 'a_H' and 'b_H' are constants that can be determined from Table 3. The finite-element results indicated that pure vertical capacity is linearly related to aspect ratio:

$$V_{ult} = a_V + b_V \left(\frac{L}{D}\right), \tag{3}$$

where 'a_V' and 'b_V' are constants that can be determined from Table 3. To determine pure moment-bearing capacity, the shape of the yield function can be described by an oblique parabola:

$$M_{ult} = a_M + b_M \left(\frac{L}{D}\right) + c_M \left(\frac{L}{D}\right)^2, \tag{4}$$

where 'a_M' , 'b_M', and 'c_M' are constants that can be determined from Table 3.

As expected, both bucket diameter and embedment length significantly affected the pure horizontal, vertical, and moment capacities of the bucket. Embedment caused pure horizontal, vertical, and moment capacities to increase. The increasing rate of pure horizontal, vertical, and moment capacities rose together with L/D ratio at different diameters. Pure horizontal capacities at bucket diameters of $D = 8$ m, 12 m, 16 m, and 20 m with an increase in aspect ratio from $L/D = 0$ to 0.25 were 3.1, 3.8, 5.9, and 7.2 times; from $L/D = 0.25$ to 0.5 were 2.1, 2.1, 1.7, and 1.95 times; from $L/D = 0.5$ to 0.75 were 1.1, 1.3, 1.2, and 1.2 times; from $L/D = 0.75$ to 1 were 1.25, 1.2, 1.2, and 1.2 times, respectively.

The increasing rate of pure vertical capacity rose as bucket diameter went up slightly at different aspect ratios in comparison with pure horizontal and moment capacity. Pure vertical capacities at bucket diameters of $D = 8$ m, 12 m, 16 m, and 20 m with an increase in

Table 3. Constants used for different functions.

Equation	Constant	$D = 8$ m	$D = 12$ m	$D = 16$ m	$D = 20$ m
(2)	a_H	1.84	2.88	8.1	9.44
(2)	b_H	11.4	26.32	49.32	83.92
(3)	a_V	22.78	45.44	64.94	94
(3)	b_V	35.08	70.28	118.73	124.53
(4)	a_M	3.96	9.92	29.18	58.1
(4)	b_M	25.12	28.57	173.46	177.09
(4)	cM	54.01	281.71	714.06	1851
(5)	$a_{d_{c_H}}$	8.56	11.78	14.49	21.11
(6)	$a_{d_{c_V}}$	1.19	1.35	2.04	1.11
(7)	$a_{d_{c_M}}$	6.42	7.02	9.31	5.23
(7)	$b_{d_{c_M}}$	13.72	24.84	32.29	25.7

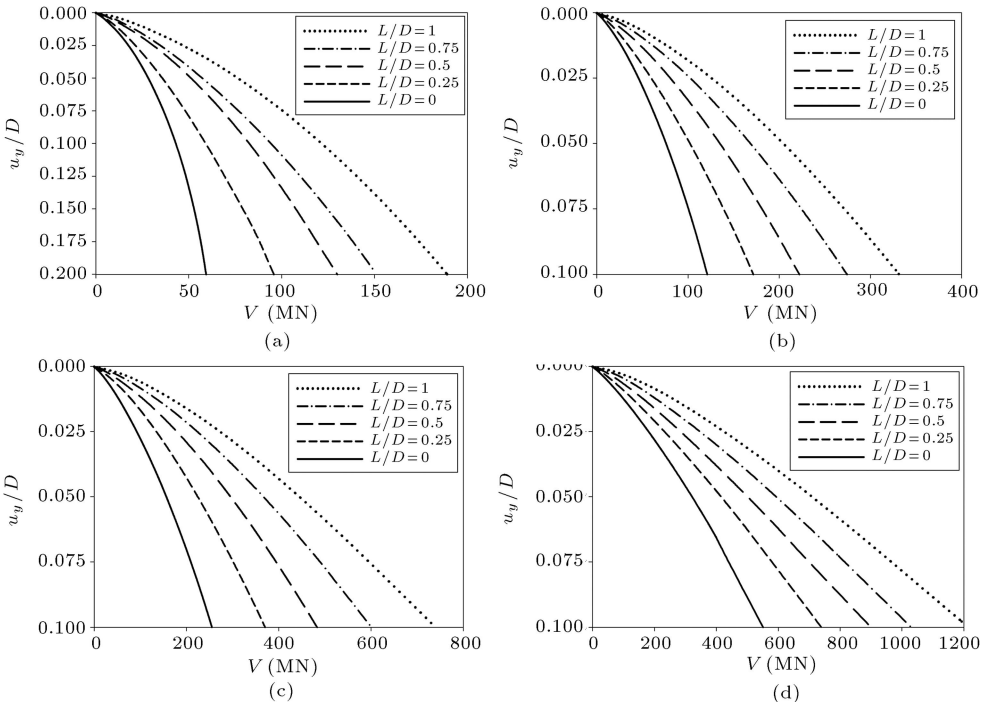

Figure 15. Settlement to diameter ratio versus pure vertical load curves at different diameters: (a) $D = 8$ m, (b) $D = 12$ m, (c) $D = 16$ m, and (d) $D = 20$ m.

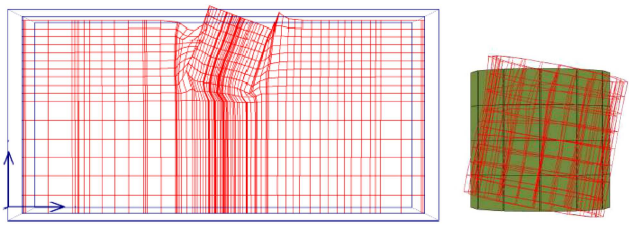

Figure 16. Deformed finite-element mesh in pure moment load at large deformations.

aspect ratio from $L/D = 0$ to 0.25 were 1.2, 1.2, 1.5, and 1.2 times; from $L/D = 0.25$ to 0.5 were 1.2, 1.35, 1.4, and 1.15 times; from $L/D = 0.5$ to 0.75 were 1.25, 1.3, 1.2, and 1.3 times; from $L/D = 0.75$ to 1 were 1.35, 1.15, 1.15, and 1.2 times, respectively.

Pure moment capacities at bucket diameters of $D = 8$ m, 12 m, 16 m, and 20 m with an increase in aspect ratio from $L/D = 0$ to 0.25 were 3.3, 3.5, 6.2, and 3.4 time; from $L/D = 0.25$ to 0.5 were 2.5, 3, 2.2, and 2.65 times; from $L/D = 0.5$ to 0.75 were 1.6, 1.8, 1.85, and 2.05 times; from $L/D = 0.75$ to 1 were 1.65, 1.75, 1.7, and 1.8 times, respectively.

To determine the normalized relationships, depth factors, that show the ratios of L/D pure bearing capacity to $L/D = 0$ pure bearing capacity (as shown below), were considered:

$$d_{c_H} = \frac{H_{ult_{(L/D)}}}{H_{ult_{(L/D=0)}}},$$

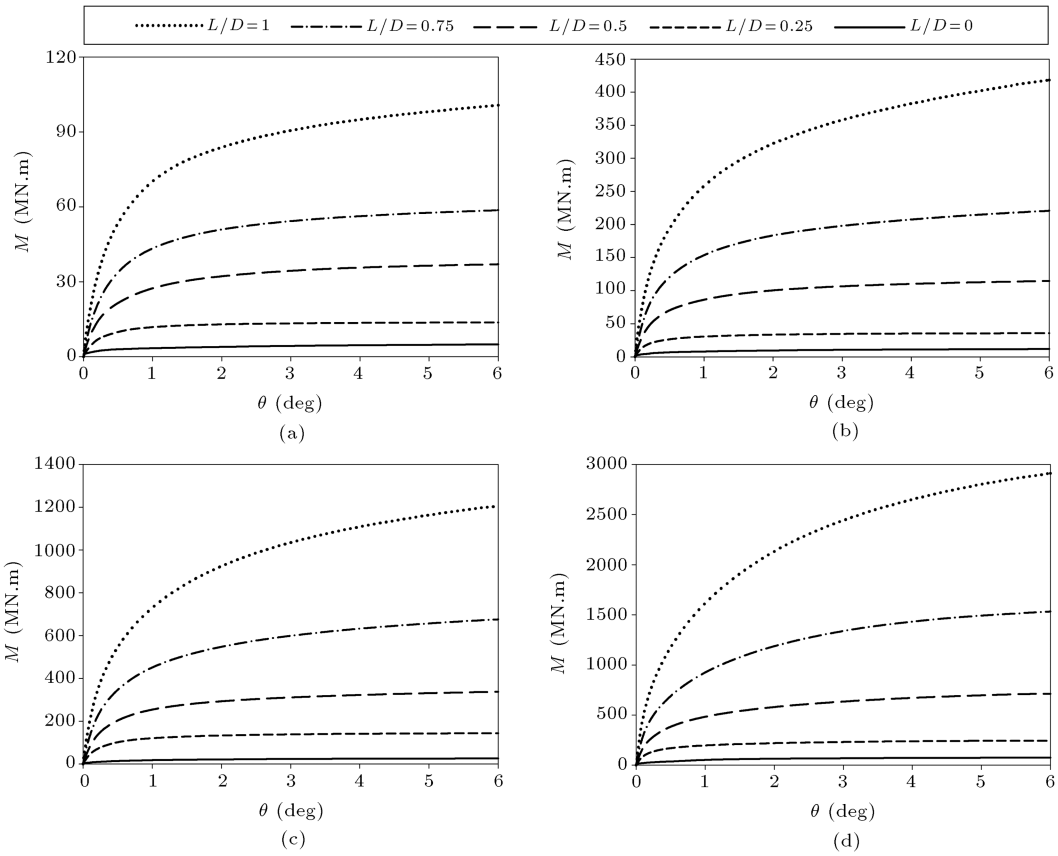

Figure 17. Pure moment-rotation curves at different diameters: (a) $D = 8$ m, (b) $D = 12$ m, (c) $D = 16$ m, and (d) $D = 20$ m.

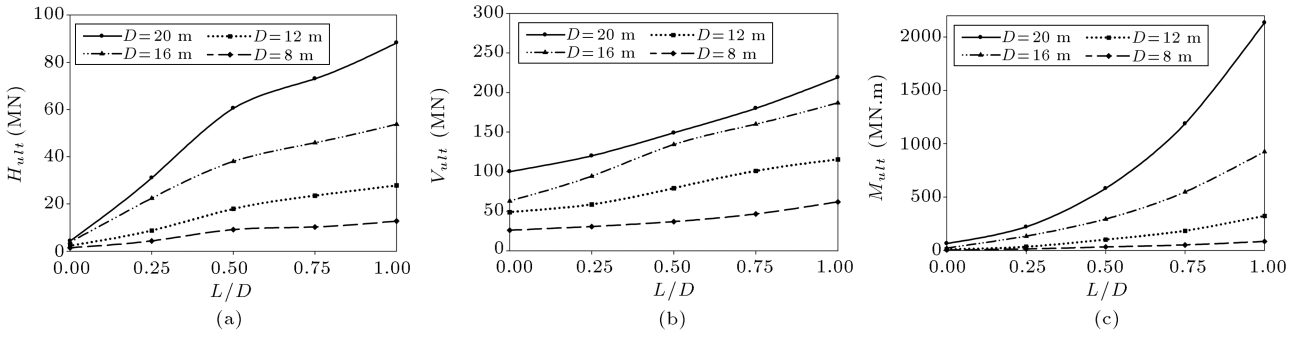

Figure 18. Pure bearing capacity as a function of aspect ratio: (a) Horizontal, (b) vertical, and (c) moment.

$$d_{c_V} = \frac{V_{ult_{(L/D)}}}{V_{ult_{(L/D=0)}}},$$

$$d_{c_M} = \frac{M_{ult_{(L/D)}}}{M_{ult_{(L/D=0)}}}.$$

Figure 19 shows variations in pure horizontal, vertical, and moment capacities of depth factors as a function of aspect ratio.

In d_{c_H} versus L/D curve, the scatters in the results were rather large, and thus, no unique function could be derived. However, by determining upper and lower bound solutions, depth factor's pure ultimate horizontal capacity could be described by the following expression:

$$d_{c_H} = \frac{H_{ult_{(L/D)}}}{H_{ult_{(L/D=0)}}} = 1 + a_{d_{c_H}} \left(\frac{L}{D}\right), \tag{5}$$

where '$a_{d_{c_H}}$' is a constant that can be determined from Table 3, although caution should be exercised when extrapolated to lower and higher diameters without additional analyses. The results of finite-element analyses in this study suggested a linear expression between normalized ultimate uniaxial vertical load and aspect ratio, which could be derived as a depth factor

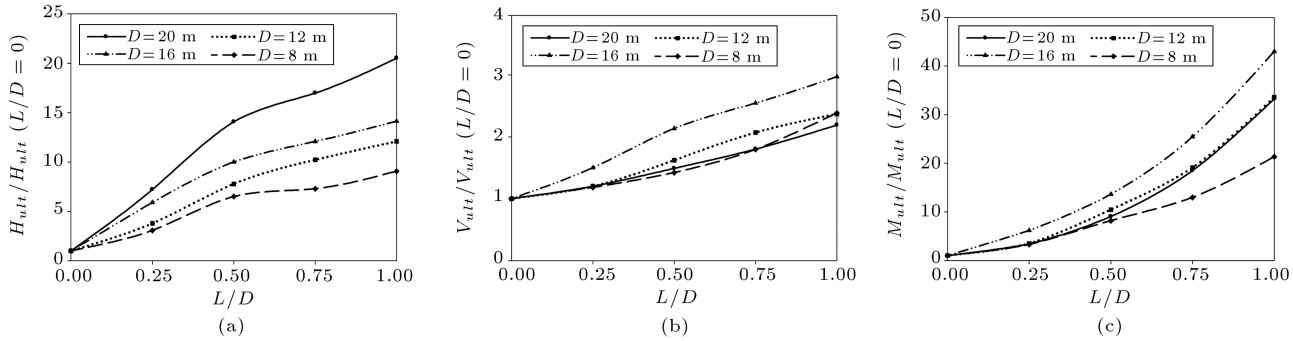

Figure 19. Normalized pure bearing capacity as a function of aspect ratio: (a) Horizontal, (b) vertical, and (c) moment.

by:

$$d_{c_V} = \frac{V_{ult_{(L/D)}}}{V_{ult_{(L/D=0)}}} = 1 + a_{d_{cV}} \left(\frac{L}{D}\right), \tag{6}$$

where '$a_{d_{cV}}$' is a constant that can be determined from Table 3. Finite-element results indicated that depth factor's pure moment capacity is related to the square of aspect ratio. Depth factor's moment capacity can be expressed by the quadratic function:

$$d_{c_M} = \frac{M_{ult_{(L/D)}}}{M_{ult_{(L/D=0)}}} = 1 + a_{d_{cM}} \left(\frac{L}{D}\right) + b_{d_{cM}} \left(\frac{L}{D}\right)^2, \tag{7}$$

where '$a_{d_{cM}}$' and '$b_{d_{cM}}$' are constants that can be determined from Table 3. One of the aims of this study was to derive ultimate loads and present them in interaction diagrams. To compare pure horizontal, vertical, and moment-bearing capacities (H_{ult}, V_{ult}, and M_{ult}) with combined bearing capacities ($H_{\max}$, $V_{\max}$, and $M_{\max}$) at $V = 0$, the horizontal loading eccentricity in a large limit with $h = 0$ m, 3 m, 5 m, 7 m, 10 m, 20 m, 40 m, 70 m, and 100 m and pure moment at $D = 16$ m were considered. Figure 20 shows failure envelope at various aspect ratios in HM plane ($V = 0$) considering the horizontal loading eccentricity.

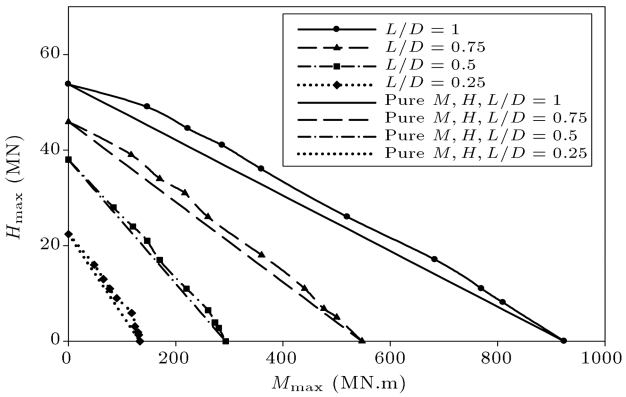

Figure 20. Failure envelope at various aspect ratios in $H - M$ plane ($V = 0$), pure loading as well as load eccentricity at $D = 16$ m.

Comparing probabilistic failure line with that of the combined failure envelope at different aspect ratios showed a curve with a slight curvature. Hence, probabilistic failure envelope line could be regarded as a combined failure envelope curve. Thus, failure envelopes presented in Figure 21 in $H - M$ plane ($V = 0$) at different diameters and aspect ratios could be a preliminary design to reach adequate bucket dimensions (L, D).

Combined bearing capacity would be likely to pass from the path presented between pure horizontal and moment-bearing capacity (such as Figure 20). Relevant studies on buckets suggested that the shape of the yield surface can be described by an oblique line in $M - H$ plane. Since wind turbines transfer high horizontal and moment loads compared to their weights of bucket foundation, VM and VH planes might be non-critical.

6. Conclusions

The main aim of the study was to determine pure horizontal, vertical, and moment-bearing capacities of bucket foundations in medium-dense sand, attributable to embedment. The study considered different methods, i.e. tangent intersection method, hyperbolic method, and limiting the deformation and rotation of bucket foundation.

Comparison made between the proposed methods showed that the following suggestions could be considered to evaluate the pure horizontal, vertical, and moment-bearing capacities of bucket foundations.

Both pure horizontal bearing capacity and pure moment capacity of the bucket foundation were defined in this numerical study as the load corresponding to a rotation of 2°. The results can be extended to the conditions of combined bearing capacity.

To determine pure vertical bearing capacity of the bucket foundation, a load corresponding to a settlement of 30 cm was considered.

To obtain pure horizontal, vertical, and moment-bearing capacities at different diameters and aspect ratios, failure envelope charts and relationships were

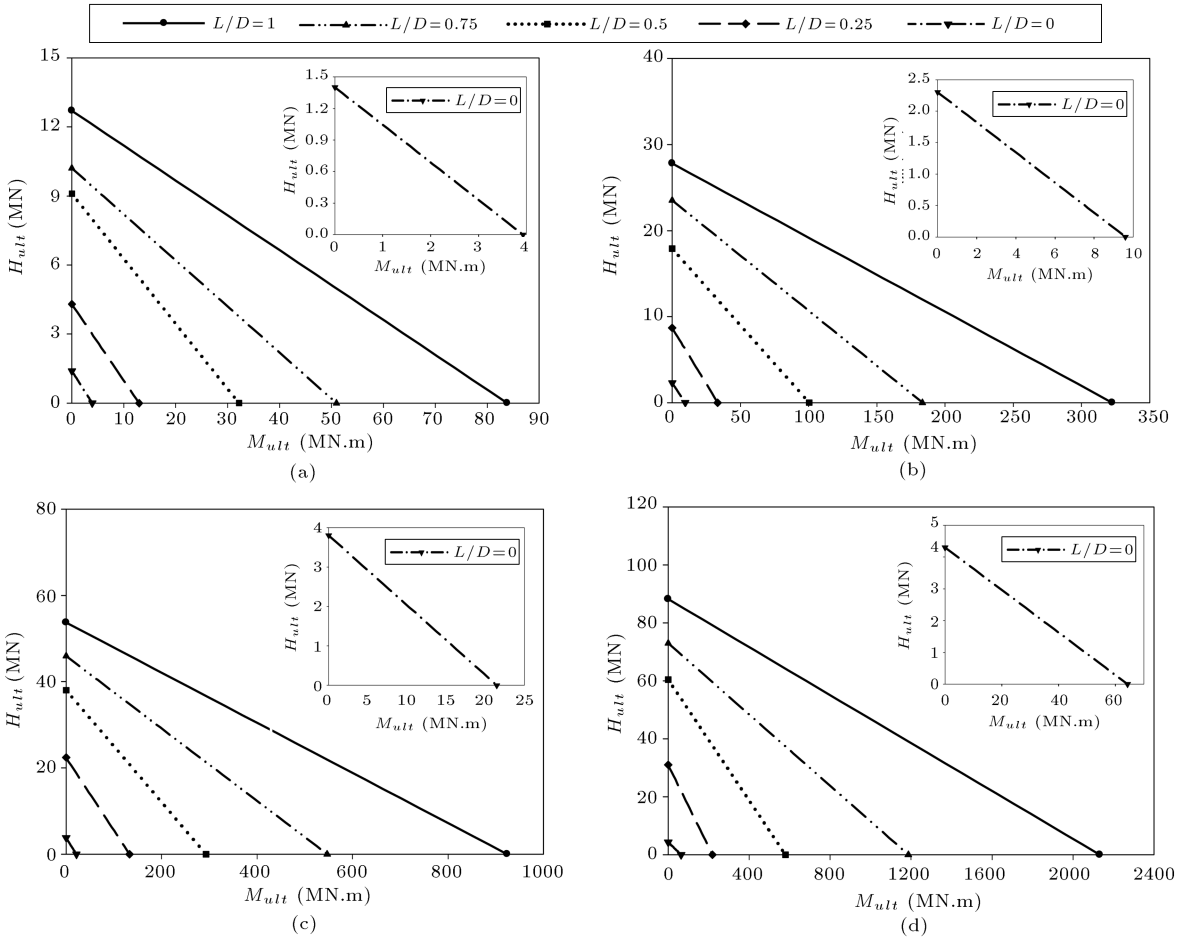

Figure 21. Probabilistic failure line at various aspect ratios in $H - M$ plane ($V = 0$) at: (a) $D = 8$ m, (b) $D = 12$ m, (c) $D = 16$ m, and (d) $D = 20$ m.

considered. On the other hand, the presented curves could be utilized in a preliminary design to evaluate suitable bucket dimensions (L, D).

The pure horizontal, vertical, and moment-bearing capacities increased as bucket diameter (D) and aspect ratio (L/D) rose at different diameters. Embedment caused the horizontal displacement, settlement, and rotation of bucket foundations to reduce significantly.

Acknowledgement

The authors would like to convey their sincere gratitude and respect for Dr. A. Barari (Postdoctoral Researcher at Virginia Tech University) for his encouragement and consideration.

References

1. Larsen, K.A. "Static Behavior of bucket foundation", PhD Thesis. Aalborg University, Denmark (2008).
2. Achmus, M., Akdag, C.T. and Thieken, K. "Load-bearing behavior of suction bucket foundations in sand", *Applied Ocean Research*, **43**, pp. 157-165 (2013).
3. Lekkakis, P. "Analysis of Skirted foundations for offshore wind turbines", PhD Thesis, National Technical University of Athens, Greece. (2012).
4. Cassidy, M.J., Byrne, B.W. and Houlsby, G.T. "Modelling the behavior of circular footings under combined loading on loose carbonate sand", *Géotechnique*, **52**(10), pp. 705-712 (2002).
5. Houlsby, G.T. and Cassidy, M.J. "A plasticity model for the behaviour of footings on sand under combined loading", *Géotechnique*, **52**(2), pp. 117-129 (2002).
6. Cassidy, M.J. "Experimental observations of the combined loading behavior of circular footings on loose silica sand", *Géotechnique*, **57**(4), pp. 397-401 (2007).
7. Gourvenec, S. and Randolph, M. "Effect of strength non-homogeneity on the bearing capacity of circular skirted foundations subjected to combined loading", *Proceedings of the Twelfth International Offshore and Polar Engineering Conference*, Kitakyushu, Japan (2002).
8. Gourvenec, S. and Randolph, M. "Bearing capacity of a skirted foundation under VMH loading", *Proceed-*

ings of OMAE03 22nd International Conference on Offshore Mechanics and Arctic Engineering, Cancun, Mexico (2003).

9. Bransby, M.F. and Yun, G.-J. "The undrained capacity of skirted strip foundations under combined loading", *Géotechnique*, **59**(2), pp. 115-125 (2009).
10. Gerolymos, N. and Gazetas, G. "Development of Winkler model for static and dynamic response of caisson foundations with soil and interface nonlinearities", *Soil Dynamics and Earthquake Engineering*, **26**, pp. 363-376 (2006).
11. Gerolymos, N. and Gazetas, G. "Winkler model for lateral response of rigid caisson foundations in linear soil", *Soil Dynamics and Earthquake Engineering*, **26**, pp. 347-361 (2006).
12. Bienen, B., Byrne, B.W., Houlsby, G.T. and Cassidy, M.J. "Investigating six-degree-of-freedom loading of shallow foundations on sand", *Géotechnique*, **56**(6), pp. 367-379 (2006).
13. Kelly, R.B., Houlsby, G.T. and Byrne, B.W. "A comparison of field and laboratory tests of caisson foundations in sand and clay", *Géotechnique*, **56**(9), pp. 617-626 (2006).
14. Gourvenec, S. "Shape effects on the capacity of rectangular footings under general loading", *Géotechnique*, **57**(8), pp. 637-646 (2007).
15. Gourvenec, S. "Failure envelopes for offshore shallow foundations under general loading", *Géotechnique*, **57**(9), pp. 715-728 (2007).
16. Gourvenec, S. "Effect of embedment on the undrained capacity of shallow foundations under general loading", *Géotechnique*, **58**(3), pp. 177-185 (2008).
17. Bienen, B., Gaudin, Ch., Cassidy, M., Rausch, L. and Purwana, O.A. "Numerical modelling of undrained capacity of hybrid skirted foundation under combined loading", *International Journal of Offshore and Polar Engineering*, **22**(4), pp. 323-329 (2012).
18. Gerolymos, N., Zafeirakos, A. and Souliotis, C. "Insight to failure mechanisms of caisson foundations under combined loading: A macro-element approach", *Second International Conference on Performance-based Design in Earthquake Geotechnical Engineering*, Taormina, Italy (2012).
19. Gerolymos, N. and Gazetas, G. "Static and dynamic response of massive caisson foundations with soil and interface nonlinearities-validation and results", *Soil Dynamics and Earthquake Engineering*, **26**, pp. 377-394 (2006).
20. Hung, L.CH. and Kim, S.R. "Evaluation of vertical and horizontal bearing capacities of bucket foundations in clay", *Ocean Engineering*, **52**, pp. 75-82 (2012)
21. Abdel-Rahman, KH. and Achmus, M. "Behavior of monopile and suction bucket foundation systems for offshore wind energy plants", *5th International Engineering Conference*, Sharm El-sheikh, Egypt (2006).
22. Panayides, S., Rouainia M. and Osman, A. "A numerical study of behavior of suction caissons in structured soil subjected to combined loads", *Ocean Engineering, Manuscript Draft*, Manuscript Number: OE-D-13-00241 (2013).
23. Larsen, K.A., Ibsen, L.B. and Barari, A. "Modified expression for the failure criterion of bucket foundations subjected to combined loading", *Can. Geotech. J.*, **50**, pp. 1-10 (2013).
24. Foglia, A., Govoni, L., Gottardi, G. and Ibsen, L.B. "Investigations on macro-element modelling of bucket foundations for offshore wind turbines", *ISSN 1901-7278 DCE Technical Memorandum*, **48** (2014).
25. Ibsen, L.B., Barari A. and Larsen, A. "Adaptive plasticity model for bucket foundations", *Journal of Engineering Mechanics*, **140**, pp. 361-373 (2014).
26. Ibsen, L.B., Larsen, K.A. and Barari, A. "Calibration of failure criteria for bucket foundations on drained sand under general loading", *Journal of Geotechnical and Geoenvironmental Engineering*, **140**(7), pp. 1-16 (2014).
27. Barari, A. and Ibsen, L.B. "Effect of embedment on the vertical bearing capacity of Bucket foundations in clay", *In Proceedings, Pan-Am CGS Geotechnical Conference*, Toronto, Ontario (2011).
28. Barari, A. and Ibsen, L.B. "Undrained response of bucket foundations to moment loading", *Applied Ocean Research*, **36**, pp. 12-21 (2012). DOI: 10.1016/j.apor.2012.01.003.
29. Barari, A. and Ibsen, L.B. "Vertical capacity of bucket foundations in undrained soil", *Journal of Civil Engineering and Management*, **20**(30), pp. 360-371 (2014).
30. Ding, H., Liu, Y., Zhang, P. and Le, C. "Model tests on the bearing capacity of wide-shallow composite bucket foundations for offshore wind turbines in clay", *Ocean Engineering*, **103**, pp. 114-122 (2015).
31. Zhang, P., Guo, Y., Liu, Y. and Ding, H. "Experimental study on installation of hybrid bucket foundations for offshore wind turbines in silty clay", *Ocean Engineering*, **114**, pp. 87-100 (2016).
32. PLAXIS user's manual, version 1.6 (2005).

Biographies

Vali Ghaseminejad was born in 1982. He earned his BSc in Civil Engineering from Islamic Azad University, Ghaemshahr Branch, Iran, in 2004. He then attended University of Mazandaran where he was awarded MSc in Geotechnical Engineering in 2009; currently, he is a student of PhDc in Geotechnical Engineering at University of Science and Research, Isfahan, Iran. His PhDc thesis is entitled "Evaluation of behavior of bucket foundations under combined loading" that is focused on the evaluation of pure and combined bearing capacities, depth factors, failure mechanisms, and normalized bearing capacity relations under pure

and combined loading. His research interests include earth dam, slope stability, and marine geotechnical engineering.

Mohammad Ali Rowshanzamir received his BSc in Civil Engineering from Isfahan University of Technology, Isfahan, Iran, in 1985, MSc in Soil Mechanics and Foundation Engineering from Amirkabir University of Technology, Tehran, Iran, in 1989, and PhD in Geotechnical Engineering from The University of New South Wales, UNSW, Sydney, Australia, in 1996. He is currently an Associate Professor at Civil Engineering Department in Isfahan University of Technology, IUT. He has published several books on Foundation Engineering, Marine Geotechnics, and Soil Mechanics (in Persian). He has received seasonal and annual awards of adorable book for publication of Marine Geotechnics (translation). He has 18 years of teaching experience in Soil Mechanics, and Foundation Engineering.